

PHYSICOCHEMICAL PROBLEMS
OF MATERIALS PROTECTION

**Corrosion Inhibition Effect of Ethyl
1-(4-chlorophenyl)-5-methyl-1*H*-1,2,3-triazole-4-carboxylate
on Aluminium Alloy in Hydrochloric Acid**

Raviprabha K^a and Ramesh S. Bhat^b, *

^aDepartment of Chemistry, Shri Madhwa Vadiraja Institute of Technology and Management, Bantakal, India

^bDepartment of Chemistry, NMAM Institute of Technology, Karkala, Nitte-574110 India

*e-mail: rameshbhat@nitte.edu.in

Received July 18, 2019; revised July 29, 2019; accepted July 10, 2020

Abstract—The inhibition efficiency of Ethyl 1-(4-chlorophenyl)-5-methyl-1*H*-1,2,3-triazole-4-carboxylate (ETC) on AA6061 Aluminium (Al) alloy in 0.1M HCl solution was tested through weight loss, potentiodynamic polarisation and electrochemical impedance spectroscopy methods. The experimental results show that the inhibition efficiency of ETC increased with an increase in inhibitors concentration and temperature. Potentiodynamic polarisation indicated that the inhibitor is mixed type. From Langmuir isotherm, it was hypothesized the adsorption of inhibitors on AA6061 alloy surface might occur by physical and chemical interaction; however, the activation energy raised suggests a chemisorption process for the interaction of the inhibitor on AA6061 alloy surface. Scanning electron microscopy was used to characterise the surface morphology of the alloy in presence and in the absence of the inhibitor.

Keywords: AA6061, corrosion, ETC, polarisation, EIS, SEM

DOI: 10.1134/S2070205120060209

1. INTRODUCTION

The corrosion of aluminium and its alloys has drawn considerable attention from many scientists because of their elevated mechanical strength, low price, low density and excellent machinability, and they have been commonly used in industrial applications, particularly in construction, electronics, packaging, storage and transportation facilities and machinery [1, 2]. Aluminium is mainly resistant to corrosion owing to its thin, adherent surface oxide film. However, aluminium and its alloy are reactive materials and are susceptible to corrosion [3]. Upon exposure to aqueous solution, a powerful adherent and constant passive oxide film is created on Al. This surface film dissolves when the metal is subjected to elevated acid or base concentrations [4]. Hydrochloric acid is generally used in industrial applications such as cleaning, etching, de-scaling etc. These processes lead to metal loss through corrosion [5]. One of the most significant techniques is to use sulfur, oxygen or nitrogen containing organic compounds as corrosion inhibitors to prevent the corrosion response and thereby decrease the rate of corrosion. Compounds with π -bonds also usually have excellent inhibitive characteristics owing to an orbital interaction with the metal surface [6]. The inhibition of such compounds is based on its molecular adsorption capacity, which iso-

lates the metal from corrosion. By chemisorption, physical adsorption or complexation, the inhibitors are attached to metal surfaces with polar groups functioning as reactive centres in the molecules [7–10].

Gabriel O. Resende, et al., [11] synthesised and studied the anticorrosion properties of Ethyl 1-(4-nitrophenyl)-5-methyl-1*H*-1,2,3-triazole-4-carboxylate on carbon steel alloy in 1 mol/L HCl solution by electrochemical and weight loss method. They showed that inhibition effectiveness was found to improve with a rise in inhibitor concentration.

In the present research, the impact of Ethyl 1-(4-chlorophenyl)-5-methyl-1*H*-1,2,3-triazole-4-carboxylate (ETC) in 0.1M HCl solution as a corrosion inhibitor for AA6061 Al alloy is explained. Weight loss technique, potentiodynamic polarization and EIS techniques were used to test alloy coupons. Taking into account the impact of temperature as well as activation and thermodynamic parameters, the mechanism of adsorption by the inhibitor was explored.

2. EXPERIMENTAL PROCEDURE

2.1. Preparation of Specimen

Corrosion studies were carried out on AA6061 alloy specimen. The composition of AA6061 Al alloy is given in Table 1. The aluminium sample was drawn

Table 1. Chemical Composition of AA 6061

Element	Cu	Mg	Si	Fe	Mn	Ti	Cr	Zn	Others	Al
wt %	0.15–0.40	0.8–1.2	0.4–0.8	0.7 Max	0.15 Max	0.15 Max	0.04–0.35	0.25 Max	0.15 Max	Balance

in the form of a cylindrical rod with an open surface region of 1.31 cm²; rest was covered with Araldite resin. Specimen was abraded with different grade emery papers. Before the experiment, the sample was washed with double distilled water, degreased in acetone, lastly dried and used for evaluation instantly.

2.2. Preparation of Medium

The acid solution (0.1M HCl) was prepared by using analytical grade reagent (Merck) of 37% HCl and double distilled water. The standardization of HCl was done with standard NaOH solution by volumetric method. From the standard solution, the required concentration of HCl (0.1M) solution was prepared as and when required. Experiments were carried out using calibrated thermostat at temperatures 303, 313 and 323 K under unstirred and aerated conditions. The inhibitive effect was studied by using 20–100 ppm of Ethyl 1-(4-chlorophenyl)-5-methyl-1*H*-1,2,3-triazole-4-carboxylate (ETC) in HCl solutions. The molecular structure of ETC is given in Fig. 1.

2.3. Methods

2.3.1. Weight loss method. The AA6061 alloy coupons of dimensions 1.5 × 2.5 × 1 cm were used for weight loss measurements. These specimens were polished with emery paper of different grades, washed with distilled water and acetone then dried. The immersion time was optimised to 6 h and was uniformly used for weight loss measurement at 303 K by weighing the specimens before and after immersing in 100 mL of 0.1M HCl in 250 mL open beaker with and without ETC. After the immersion period the specimens were removed from the medium, cleaned by wiping the coupons with tissue paper, washed with distilled water followed by acetone, dried and then

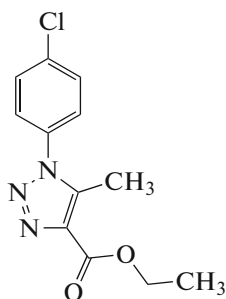


Fig. 1. Chemical structure of Ethyl 1-(4-chlorophenyl)-5-methyl-1*H*-1,2,3-triazole-4-carboxylate molecule.

weighed. The inhibition efficiency and corrosion rate were calculated using Eqs. (1) and (2).

$$IE(\%) = \frac{W_o - W_{in}}{W_o} \times 100, \quad (1)$$

$$C.R.(\text{mm/y}) = 87.6 \Delta w / Atd. \quad (2)$$

Where Δw is weight loss, A is area of the specimen in cm², t is the immersion time in hours, d is density of Aluminium in g/cm³; W_o and W_{in} are the weight loss values without and with inhibitors respectively.

2.3.2. Electrochemical studies. Electrochemical measurements of AA6061 alloy was carried out by using Potentiostat (CH604 E-series, U.S. model with CH-instrument beta software). Both polarization studies and electrochemical impedance measurements (EIS) are carried out using conventional three-electrode glass cell with platinum counter electrode and saturated calomel electrode as reference and AA6061 alloy specimen as working electrode. The freshly polished specimen was exposed to corrosive medium of 0.1M HCl in the presence and absence of ETC at different temperatures and allowed to establish steady state open circuit potential. Potentiodynamic polarization measurements were done by polarizing the specimen from –250 mV cathodically to +250 mV anodically with respect to OCP with a scan rate of 1m Vs⁻¹ and the potentiodynamic current–potential ($I-E$) plots were recorded. The experiments are performed at different temperatures using calibrated Thermostat. Corrosion potential (E_{corr}) and corrosion current density (i_{corr}) are recorded, from which corrosion rate (C.R.) and percentage inhibition efficiency (% IE) are calculated. The EIS studies were done by impressing 10 mV of small amplitude AC signal on the open-circuit potential with a frequency range from 10000 to 0.01 Hz. Nyquist plots were used for the analysis of impedance data to assess corrosion characteristics. The charge transfer resistance (R_{ct}) and the double layer capacitance (C_{dl}) were deduced from the simulation of impedance data with Randles equivalent circuit using ZSimpWin version 3.21 software.

2.3.3. Surface morphology studies. Surface morphology study of AA6061 Al alloy was carried out by using analytical scanning electron microscope (JEOL JSM-6380L), in the magnification of 1000X. Surface morphology of the metal sample was obtained by immersing the specimen in hydrochloric acid medium for 6 h without and with the presence of 100 ppm of the ETC in 0.1M HCl.

Table 2. Results of weight loss, corrosion rate and inhibition efficiencies at different concentrations of ETC at 303 K

Concentration of ETC in ppm	Weight loss, mg	C.R., mm/y	IE, %
Blank	15.5	38.39	—
20	3.8	9.41	75.48
40	3.4	8.42	78.06
60	2.8	6.93	81.93
80	2.5	6.19	83.87
100	2.4	5.94	84.51

3. RESULTS AND DISCUSSION

3.1. Weight Loss Method

Corrosion inhibition effectiveness of ETC is calculated after 6 h of immersion at 303 K by gravimetric weight loss technique. The weight loss, corrosion rate and inhibition efficiencies are shown in Table 2. The inhibition effectiveness enhanced with a four-fold rise in the inhibitor concentration from 75.48 to 84.51%. At 100 ppm, ETC has showed the maximum inhibition efficiency of 84.51%. Figure 2 indicates variation of inhibition efficiency and loss of weight with concentration. Nearly the same effectiveness was achieved above this concentration; therefore, it is regarded to be the optimum concentration for maximum effectiveness of inhibition.

3.2. Potentiodynamic Polarization (PDP) Measurements

The impact of concentration of inhibitor on AA6061 corrosion rate has been investigated. Figure 3 represents potentialodynamic polarization plots in 0.1 M HCl solution at 323K for corrosion of AA6061 alloy in the presence of variable inhibitor levels. The polarization experiments acquired electrochemical parameters such as corrosion current density (i_{corr}), corrosion potential (E_{corr}). The corrosion rate (C.R.) in mm/y was obtained by using Eq. (3).

$$C.R. = \frac{3270 M i_{\text{corr}}}{\rho Z} \quad (3)$$

Where, 3270 is a constant that defines the unit of corrosion rate, ρ is the density of the corroding material (2.7 g/cm^3), M is the atomic mass of metal (27), Z is the number of electrons transferred per metal atom [12]. The percentage inhibition efficiency of the inhibitor may be calculated by using Eq. (4).

$$\eta = \frac{i_{\text{corr}(o)} - i_{\text{corr}(in)}}{i_{\text{corr}(o)}} \times 100. \quad (4)$$

Where $i_{\text{corr}(o)}$ and $i_{\text{corr}(in)}$ are the corrosion current densities in the absence and in the presence of the inhibitor respectively. The results of potentiodynamic polarization measurement for the corrosion of AA6061 Al alloy in 0.1M hydrochloric acid containing various concentrations of inhibitor at different temperatures is

shown in Table 3. It clearly shows that the corrosion current density (i_{corr}) and corrosion rate (C.R.) values decrease in the presence of different concentrations of inhibitor. Hence, the inhibition efficiency increases with an increase in concentration inhibitor. Figure 4 shows the effect of concentration of ETC and temperature on corrosion rate and inhibition efficiency. At higher temperature i.e. at 323 K, highest corrosion rate has been found in blank sample shown in Table 3, but the inhibition efficiency was (86.36%) highest at 323K. This is mainly because of adsorption of the inhibitor on the AA6061 alloy surface. The adsorbed inhibitor molecule creates a protective self barrier between the aluminium surface and the aggressive medium [13].

It is reported in literature [13–15] that, if the corrosion potential (E_{corr}) value of the inhibited solution is less than $\pm 85 \text{ mV}$ with respect to uninhibited solution, the inhibitor can be considered as distinctively as anodic and cathodic inhibitor. However, in the study the maximum displacement was much less than $\pm 85 \text{ mV}$. This suggests that ETC may act as a mixed type inhibitor, with predominance of anodic inhibition. In Fig. 3 the shapes of polarization curves in the absence and presence of the inhibitor are similar, this suggested that the hydrogen evolution is activated-controlled and it does not alter the mechanism of

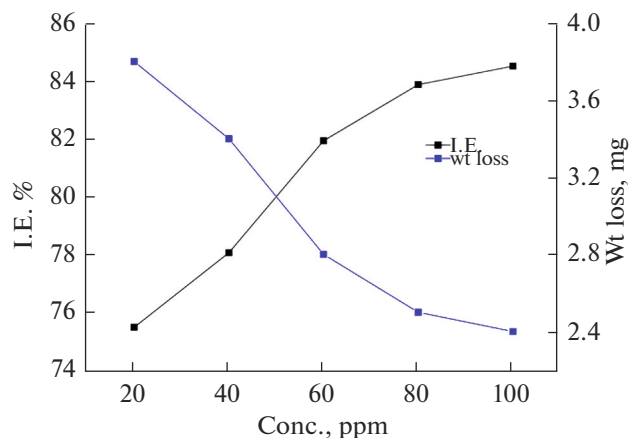


Fig. 2 Variation of inhibition efficiency and weight loss with concentration.

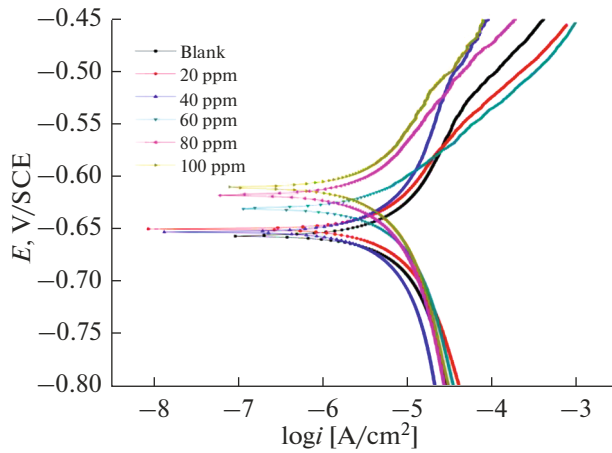


Fig. 3. Potentiodynamic polarisation plots for AA6061 Al alloy in 0.1M HCl with various concentrations of ETC at 323 K.

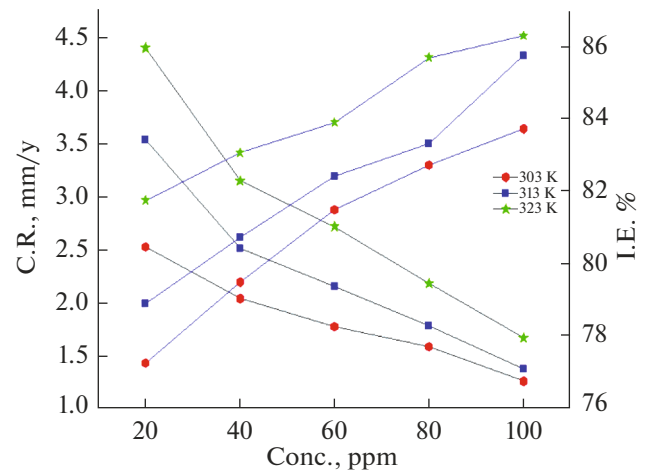


Fig. 4. The effect of concentration of ETC and temperature on corrosion rate and inhibition efficiency.

reduction reaction [2]. Slopes of anodic (β_a) and cathodic (β_c) Tafel lines did not vary significantly with increase in inhibitor concentration, which indicates that the hydrogen evolution is activation-controlled and the presence of inhibitor does not change the mechanism of inhibition. The added inhibitor stops the anodic reaction and supports for the passivation of oxide film on the metal surface. The inhibitor impairs anodic oxidation process and also impedes cathodic

hydrogen liberation reaction [16]. This proves that the organic inhibitor functions as mixed type inhibitor.

3.3. Electrochemical Impedance Spectroscopy (EIS) Measurements

Nyquist plots for the corrosion inhibition of AA6061 alloy in 0.1M HCl medium at various concentration of ETC at 323K as shown in Fig. 5. The impedance spectra are consisted of capacitive loops at higher

Table 3. Results of Tafel polarisation studies on AA6061 Al alloy in 0.1M HCl solution containing various concentrations of inhibitor

Temp, K	Concentration, ppm	$-E_{\text{corr}}$, mV	β_c , mV	β_a , mV	i_{corr} , mA/cm ²	C.R., mm/y	IE, %
303	Blank	711	139.7	127.4	4.01	4.95	—
	20	710	137.9	121.1	0.91	2.542	77.31
	40	678	135.3	131.4	0.82	2.055	79.55
	60	653	130.0	133.4	0.74	1.791	81.55
	80	658	122.9	130.6	0.69	1.604	82.79
	100	643	104.5	134.7	0.65	1.277	83.79
313	Blank	704	168.8	133.8	6.56	7.612	—
	20	698	166.9	131.7	1.38	3.552	78.96
	40	663	174.9	127.5	1.26	2.528	80.79
	60	659	168.5	121.8	1.15	2.174	82.47
	80	653	154.0	129.5	1.09	1.801	83.38
	100	647	138.7	116.7	0.93	1.391	85.82
323	Blank	657	376.7	115.0	8.36	8.937	—
	20	650	472.6	128.1	1.52	4.417	81.81
	40	653	349.6	123.5	1.41	3.166	83.13
	60	631	419.7	121.3	1.34	2.735	83.97
	80	618	434.5	127.0	1.19	2.196	85.76
	100	610	435.4	120.8	1.14	1.684	86.36

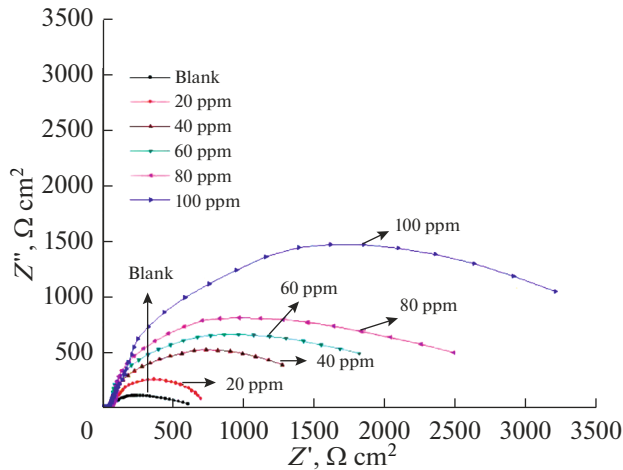


Fig. 5. Nyquist plot for corrosion of AA6061 Al alloy in 0.1M HCl with various concentrations of ETC at 323 K.

frequency and inductive loops at lower frequency. The presence of depressed semicircle in Nyquist plot across the studied frequency range indicates that a charge transfer process mainly controls the corrosion of aluminium.

The data obtained from EIS studies gives the information about the type of electrochemical process occurred at electrode/electrolyte interface. Nyquist plots were deviated semicircles due to the frequency dispersion of interfacial impedance, attributable to the roughness and non-homogeneity of the electrode surface and to the adsorption of the inhibitor and formation of porous layers [17]. The impedance spectra showed a semicircle which indicates that corrosion is mainly controlled by charge transfer process [18]. The Nyquist plot obtained for the corrosion control of AA6061 Al alloy shows that the diameter of the capacitive loop increased with increase in the inhibitor concentration, this increase in the diameter is due to decrease on the corrosion rate by the adsorption of the inhibitor molecule onto the surface of the metal.

The impedance parameters are analysed by fitting a suitable equivalent circuit to the Nyquist plots using ZSimpWin software version 3.21. Figure 6 shows the electrical equivalent circuit, which was used to simulate the impedance plot for AA6061 Al alloy. The equivalent circuit consists of nine elements. They are solution resistance (R_s) and charge transfer resistance (R_{ct}), inductive resistance (R_L) and the inductive element (L). The CPE (constant phase element, Q) is parallel to the series of capacitors C_1 and C_2 and also parallel to the series of resistor R_1 , R_2 , R_L and R_{ct} . R_L is parallel to L inductor. The parallel circuit of a resistor is attributed for oxide film due to the ionic conduction in the oxide film and the capacitance due to its dielectric properties. The double layer capacitance (C_{dl}) and

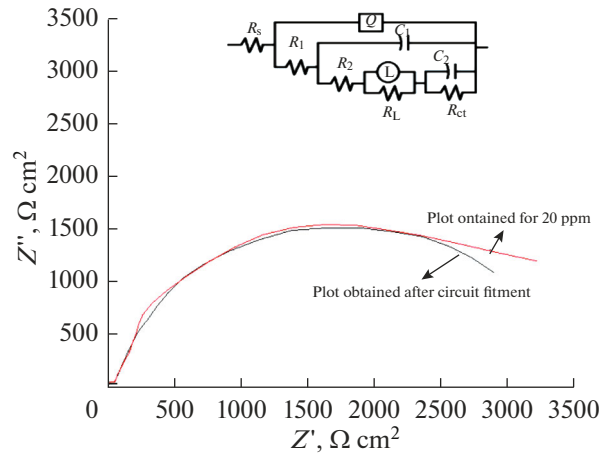


Fig. 6. (a) Electrical equivalent circuit used to fit impedance data, (b) curves obtained from experimental data and from circuit fitment.

polarization resistance (R_p) can be calculated by using equations

$$R_p = R_1 + R_2 + R_L + R_{ct}, \quad (5)$$

$$C_{dl} = C_1 + C_2. \quad (6)$$

The EIS parameters obtained are shown in Table 4. The CPE impedance is calculated using Eq. (7) [19].

$$Z = A^{-1}(i\omega)^{-n}. \quad (7)$$

Where A is proportionality constant, ω is the angular frequency, i is imaginary number and n is exponent related to the phase shift. If the value of $n = 1$, the CPE behaves like an ideal capacitor. The correlation in the capacitance to its real value is calculated using Eq. (8) [20].

$$C_{dl} = \frac{1}{2\pi f_{max} R_{ct}}. \quad (8)$$

Where f_{max} is the frequency at which the imaginary component of impedance is maximum and R_{ct} is the charge transfer resistance. The results obtained from EIS are listed in the Table 4. Measured C_{dl} value decreased with increase in concentrations of inhibitor at all temperatures. The decrease in C_{dl} values resulted from the increase in electrical double layer at the metal solution interface. Further decrease in the C_{dl} values is caused by the gradual replacement of water molecules by inhibitor molecules. The polarization resistance (R_p) values are varies inversely with corrosion current density (i_{corr}). The inhibition efficiency was obtained using Eq. (9)

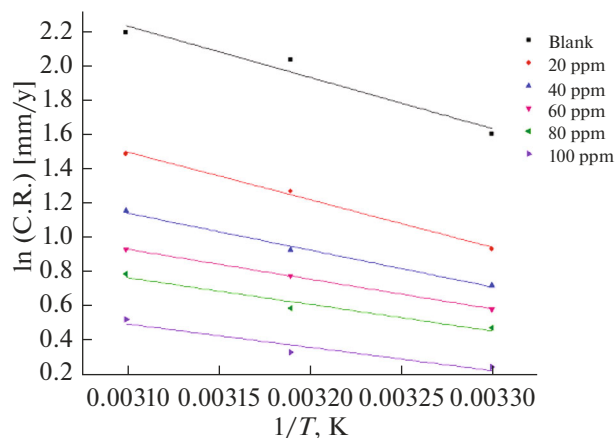
$$IE(\%) = \frac{R_p(inh) - R_p}{R_p(inh)} \times 100. \quad (9)$$

R_p and $R_p(inh)$ are the polarization resistance in the absence and in presence of the inhibitor. R_p values

Table 4. Electrochemical impedance values of AA6061 in 0.1M HCl solution containing different concentrations of ETC at different temperatures

Temperature, K	Concentration, ppm	R_p , $\Omega \text{ cm}^2$	C_{dl} , μF	IE, %
303	Blank	426	30.30	–
	20	1898	24.52	77.56
	40	2114	21.44	79.84
	60	2252	17.56	81.08
	80	2397	13.78	82.23
	100	2510	10.65	83.02
313	Blank	525	25.50	–
	20	2396	18.61	78.08
	40	2651	16.63	80.19
	60	2898	15.12	81.88
	80	3179	11.00	83.49
	100	3542	9.46	85.18
323	Blank	634	16.70	–
	20	3252.2	9.56	80.51
	40	3588.2	9.39	82.33
	60	3933.8	8.44	83.88
	80	4268.7	5.00	85.14
	100	4644.7	4.65	86.35

increased with increase in the concentration of the inhibitor. This results in lowering the value of double layer capacitance (C_{dl}), indicates that the charge transfer process is mainly controlling the corrosion process.

**Fig. 7.** Arrhenius plots for the corrosion inhibition of AA6061 in 0.1M HCl containing different concentrations of ETC.

3.4. Effect of Temperature

The effect of temperature on the corrosion rate of AA6061Al alloy in 0.1M HCl and inhibition efficiency of ETC is studied at different temperatures in the range 303–323 K from which kinetic and thermodynamic parameters for the corrosion inhibition were calculated. The corrosion activation energy (E_a) in presence and in absence of inhibitor and dependence of inhibitor's adsorption on temperature can interpret the adsorption mechanism. The energy of activation is calculated using the Arrhenius equation (10) [21, 22].

$$\ln(\text{C.R.}) = A - \frac{E_a}{RT} \quad (10)$$

Where A is Arrhenius pre-exponential constant, R is the universal gas constant and T is absolute temperature. The plot of $\ln(\text{C.R.})$ versus $1/T$ gave a straight line with slope equal to E_a/R from which the activation energy values for both corrosion and inhibition processes were calculated. The Arrhenius plots are shown in Fig. 7.

The enthalpy (ΔH) and entropy (ΔS) of activation for the metal dissolution process are determined using the transition state equation (11).

$$\text{C.R.} = \frac{RT}{Nh} \exp\left(\frac{\Delta S}{R}\right) \exp\left(\frac{-\Delta H}{RT}\right) \quad (11)$$

Where h is Plank's constant and N is Avogadro's number. A plot of $\ln(C.R./T)$ versus $1/T$ gave a straight line shown in Fig. 8 with slope = $(\Delta H/R)$ and intercept = $\ln \frac{RT}{Nh} \exp\left(\frac{\Delta S}{R}\right)$. The calculated values of activation parameters are given in Table 5.

Energy of activation (E_a) of inhibited solution is decreased with increase in inhibitor concentration. This decrease in the E_a value of the inhibited solution is suggestive of chemical adsorption of inhibitor on the surface of the metal [20, 23]. Chemisorption process involves charge transfer from the inhibitor molecule to the metal surface to form coordinate type of bond. The large negative values of entropy of activation in the absence and presence of the inhibitor implies that the activated complex in the rate determining step is an association complex rather than dissociation [24], resulting in a decrease in the randomness on going from the reactants to the activated complex [25].

3.5. Adsorption Isotherm

The degrees of surface coverage θ obtained from potentiodynamic polarisation were fitted to Langmuir, Temkin, Frumkin and Flory-Huggins isotherms. If the linear regression coefficient (R^2) and slopes are close to 1 then the best fitment is Langmuir pattern. Equation (12) represents Langmuir's adsorption isotherm for monolayer chemisorption process.

$$\frac{C_{inh}}{\theta} = \frac{1}{K} + C_{inh} \quad (12)$$

Where K represents the equilibrium constant for metal-inhibitor interaction, C_{inh} is inhibitor concentration and θ is surface coverage. The plot of C_{inh}/θ versus C_{inh} was a straight line with intercept $1/k$ shown in Fig. 9. Further the standard free energy change $-\Delta G_{ads}^\circ$ values for the adsorption are calculated using Eq. (13).

$$K = \frac{1}{55.5} \exp\left(-\frac{\Delta G_{ads}^\circ}{RT}\right) \quad (13)$$

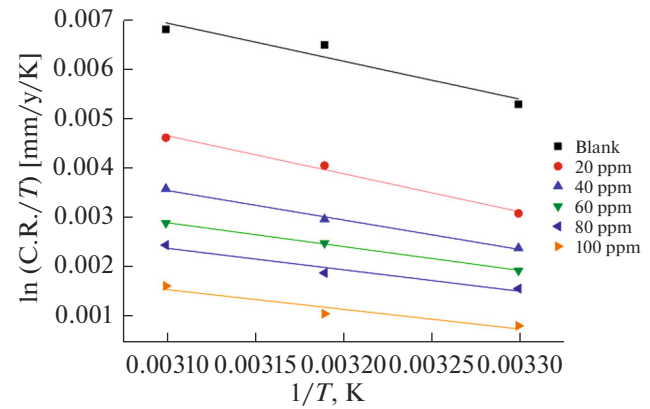


Fig. 8. Plots of $\ln(C.R./T)$ vs. $1/T$ for the corrosion inhibition of AA6061 in 0.1M HCl containing different concentrations of ETC.

Where K is the equilibrium constant, R is the universal gas constant and T is the absolute temperature and 55.5 is the concentration of water in solution in mol/dm^3 . Fig. 10 represents the plot of $-\Delta G_{ads}^\circ$ versus T . The standard enthalpy of adsorption (ΔH_{ads}°) and standard entropy of adsorption (ΔS_{ads}°) were calculated from the slope and intercept of the straight line respectively and are shown in the Table 6. The negative values of $-\Delta G_{ads}^\circ$ ensured the spontaneity of adsorption process and stability of the adsorbed layer on the alloy. Generally $-\Delta G_{ads}^\circ$ are around -20 kJ/mol or lower, then it is physisorption and if the values are more negative than -40 kJ/mol involve sharing of charge or transfer of charge from the inhibitor molecule to the metal surface to form a coordinate bond (chemisorption) [26]. In the present case, $-\Delta G_{ads}^\circ$ values are above -40 kJ/mol and ΔH_{ads}° is positive indicating that adsorption of ETC on the AA6061 alloy surface is attributable to chemisorption. Negative ΔS_{ads}° values indicate that the decrease in disordering takes place on going from reactant to adsorbed species.

Table 5. Activation parameters for the corrosion of AA6061 in 0.1M HCl containing different concentrations of ETC

Inhibitor concentration, ppm	E_a , kJ/mol	ΔH , kJ/mol	$-\Delta S$, J/mol K
Blank	24.85	63.85	197.29
20	23.05	63.79	197.30
40	17.88	49.50	197.35
60	14.44	39.99	197.39
80	12.88	35.99	197.41
100	11.29	33.00	197.43

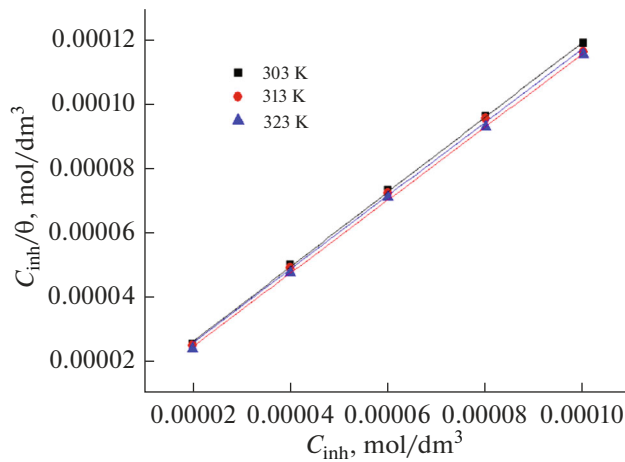
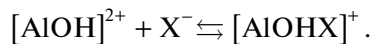
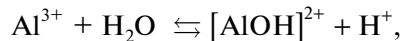
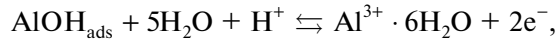


Fig. 9. Langmuir adsorption isotherms for the adsorption of ETC on AA6061 Al alloy in 0.1M HCl at different temperatures.

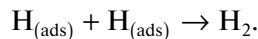
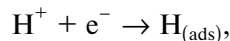
4. INHIBITION MECHANISM

According to Pilling-Bedworth rule, Aluminium reacts with Oxygen to form aluminium oxide which protects the metal from corrosion in neutral medium. But when Aluminium is exposed to acidic medium the following reactions takes place:

Anodic reaction-



Cathodic reaction-



So the metal undergoes dissolution at anode and at cathode hydrogen liberation takes place. An effective inhibitor alters the rate of metal dissolution and thereby controls corrosion process. In the present study the inhibitive action of ETC can be explained on the basis of available lone pairs of electrons on N, O atoms and π electron interaction of the benzene

Table 6. Thermodynamic parameters for the adsorption of ETC on AA6061 surface in 0.1M HCl at different temperatures

Temp, K	$\Delta G_{\text{ads}}^\circ$, kJ/mol	$\Delta S_{\text{ads}}^\circ$, kJ/mol/K	$\Delta H_{\text{ads}}^\circ$, kJ/mol
303	42.03		
313	43.25	183.2	13.7
323	45.70		

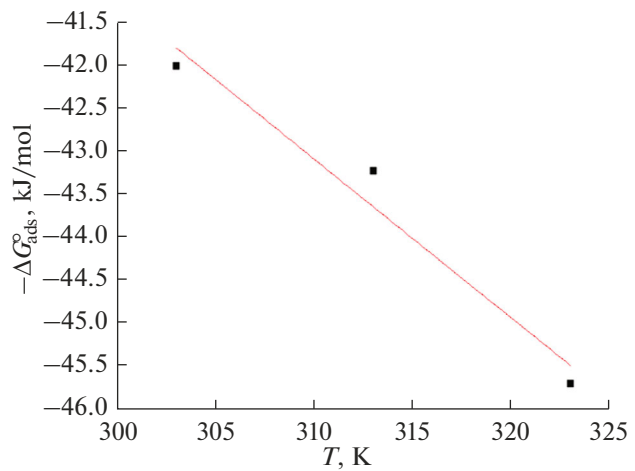


Fig. 10. Plot of $-\Delta G_{\text{ads}}^\circ$ versus T for the adsorption of ETC on AA6061 in 0.1M HCl.

nucleus with unshared p electrons of aluminium atoms. Lone pair of electrons on nitrogen and oxygen is readily available for sharing with metal atoms to form a native covalent bond. Hence, the adsorbed inhibitor will cover and protect the metal surface from the corrosion [27].

As far as the inhibition process is concerned, it is generally assumed that adsorption of the inhibitor at the metal/solution interface is the first step in the action mechanism of the inhibitors in aggressive acid media. The adsorption may be the result of one or more of three types of interactions, namely; electrostatic attraction between charged molecules and charged metal, coordination of the unshared pairs of electron on the molecule to the metal atom, and involvement of π electrons of the inhibitor molecule in coordination process [22]. Chemical adsorption process is suggested because the metal surface is protected due to the formation of co-ordinate bond between the metal and the inhibitor molecule. Formation of protective film on the metal surface is also confirmed by SEM image.

5. SCANNING ELECTRON MICROSCOPY

SEM investigations were conducted to distinguish between the surface morphology of AA6061 Al alloy after immersion in 0.1 M HCl in the presence and lack of an inhibitor for about 4 h. Figure 11a shows the freshly polished alloy surface, scratches were seen possibly due to abrasion with emery sheets. Figure 11b depicts the formation of pits and accumulation of corrosion products due to acid attack. Figure 11c confirms that inhibitor protects the alloy against corrosion through the formation of protective film when kept in 100 ppm of ETC for 4 h in acidic medium.

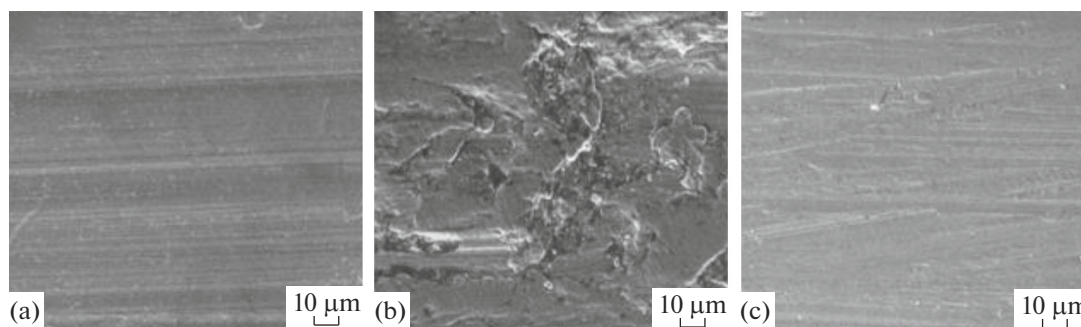


Fig. 11. SEM images of 6061Al (a) AA606 polished surface (b) AA6061 + 0.1M HCl (c) AA6061 + 0.05M HCl + ETC.

6. CONCLUSION

1. ETC has shown good inhibition effectiveness for the corrosion of AA6061 alloy in 0.1M HCl and inhibition efficiency increased on increasing the concentration of the inhibitor and temperature.

2. EIS measurements showed increase in R_p value and decrease in double layer capacitance with increase in inhibitor concentration, suggesting the adsorption of ETC on the surface of AA6061 alloy.

3. Adsorption process followed Langmuir adsorption isotherm.

4. Inhibitor acted as potential compound by controlling metal dissolution and hydrogen liberation, thereby ETC emerged as mixed type of inhibitor.

5. Scanning Electron Microscopy (SEM) shows a smoother surface for inhibited alloy due to formation of protective film.

CONFLICT OF INTEREST

The authors declare that they have no conflicts of interest.

REFERENCES

1. Fakrudeena, S.P., Ananda Murthy, H.C., and Bheema Raju, V., *J. Chil. Chem. Soc.*, 2012, vol. 57, p. 1364.
2. Rosliza, R., Senin, H.B., and Wan Nik, W.B., *Colloids Surf.*, 2008, vol. 312 p. 185.
3. Badawy, W.A., Al-Kharafi, F.M., and El-Azab, A.S., *Corros. Sci.*, 1999, vol. 41, p. 709.
4. Ergun, U., Yuzer, D., and Emregul, K.C., *Mater. Chem. Phys.*, 2008, vol. 109, p. 492.
5. Oguzie, E.E., Onuoha, G.N., and Ejike, E.N., *Pigm. Resin Technol.*, 2007, vol. 36, p. 44.
6. Noor, E.A., *Mater. Chem. Phys.*, 2009, vol. 114, p. 533.
7. Ahamad, I. and Quraishi, M.A., *Corros. Sci.*, 2009, vol. 51, p. 2006.
8. Zhang, Q.B. and Hua, Y.X., *Electrochim. Acta*, 2009, vol. 54, p. 1881.
9. Quraishi, M.A., Sardar N., and Ali, H., *Corros. Sci.*, 2002, vol. 58, p. 317.
10. Harvey, T.G., Hardin, S.G., Hughes, A.E., and Muster, T.H., *Corros. Sci.*, 2011, vol. 53, p. 2184.
11. Resende, G.O., Teixeira, S.F., Figueiredo, I.F., Godoy, A.A., Lougon, D.J.F., Cotrim, B.A., and De Souza, F.C., *Int. J. Electrochem.*, 2019, vol. 2019, article ID 6759478.
12. Fontana, M.G., *Corrosion Engineering*, Singapore: McGraw-Hill, 1987.
13. Charitha, B.P. and Rao, P., *Indian J. Mater. Environ. Sci.*, 2017, vol. 8, p. 78.
14. Ferreira, E.S., Giancomelli, C., Giacomelli, F.C., and Spinelli, A., *Mater. Chem. Phys.*, 2004, vol. 83, p. 129.
15. Li, W.H., He, Q., Pei, C.L., and Hou, B.R., *J. Appl. Electrochem.*, 2008, vol. 38, p. 289.
16. Lebrini, M., Robert, F., Blandinieres, P.A., and Roos, C., *Int. J. Electrochem. Sci.*, 2011, vol. 6, p. 2443.
17. El Maghraby, A.A., *Open Corros. J.*, 2009, vol. 2, p.189.
18. Abiola, O.K. and Otaigbe, J.O.E., *Corros. Sci.*, 2008, vol. 50, p. 242.
19. Soltani, N., Behpour, M., Ghoreishi, S.M., and Naeimi, H., *Corros. Sci.*, 2010, vol. 52, p.1351.
20. Ashassi-Sorkhabi, H., Shaabani, B., and Seifzadeh, D., *Appl. Surf. Sci.*, 2005, vol. 239, p. 154.
21. Khedr, M.G.A. and Lashien, M.S., *Corros. Sci.*, 1992, vol. 33, p. 137.
22. Rehim, S.S.A., Hassan, H.H., and Amin, M.A., *Mater. Chem. Phys.*, 2001, vol. 70, p. 64.
23. Osman, M.M., El-Ghazawy, R.A., and Al Sabagh, A.M., *Mater. Chem. Phys.*, 2003, vol. 80, p. 55.
24. Hamdy, A. and El Gendy, N.S., *Egypt. J. Pet.*, 2013, vol. 22, p. 17.
25. Soltani, N., Behpour, M., Ghoreishi, S.M., and Naeimi, H., *Corros. Sci.*, 2010, vol. 52, p. 1351.
26. Kadhum, A.A.H., Mohamad, A.B., Hamed, L.A., Al-Amiery, A.A., San, N.H., and Musa, A.Y., *Materials*, 2014, vol. 7, p. 4335.
27. Zucchi, F., Grassi, V., Frignani, A., Monticelli, C., and Trabaneli, G., *J. Appl. Electrochem.*, 2005, vol. 36, p. 195.